The Effects of Manganese Dopant Content and Calcination Temperature on Properties of Titania-Zirconia Composite

Muhamad Imam Muslim[1], Rian Kurniawan[2], Mokhammad Fajar Pradipta[1], Wega Trisunaryanti[1], and Akhmad Syoufian[1*]

[1]*Department of Chemistry, Faculty of Mathematics and Natural Sciences, Universitas Gadjah Mada, Sekip Utara, 55281 Yogyakarta, Indonesia*

[2]*Institute of Chemical Technology, Universität Leipzig, Linnéstr. 3, 04103 Leipzig, Germany*

* ***Corresponding author:***

email: akhmadsyoufian@ugm.ac.id

Received: December 5, 2020
Accepted: March 24, 2021

DOI: 10.22146/ijc.61900

Abstract: *The effects of dopant content and calcination temperature on Mn-doped TiO_2-ZrO_2 structure and properties were successfully investigated. Composite of Mn-doped titania-zirconia was synthesized by sol-gel method. Titanium(IV) isopropoxide was used as the precursor of TiO_2, while zirconia powder was used as another semiconductor. $MnCl_2{\cdot}4H_2O$ was used as the source of dopant in this study. Various amounts of manganese were incorporated into TiO_2-ZrO_2 and calcination was performed at temperatures of 500, 700 and 900 °C. Synthesized composites were characterized by Fourier-transform infrared spectroscopy (FTIR), specular reflectance UV-Vis spectroscopy (SR UV-Vis), X-ray diffraction method (XRD) and scanning electron microscopy equipped with X-ray energy dispersive spectroscopy (SEM-EDX). The results showed that Mn-doped TiO_2-ZrO_2 with the lowest bandgap (2.78 eV) was achieved with 5% of Mn dopant and calcined at 900 °C, while Mn-doped TiO_2-ZrO_2 with the highest bandgap (3.12 eV) was achieved with 1% of Mn dopant content calcined at 500 °C.*

Keywords: *Mn-doped TiO_2-ZrO_2; bandgap; manganese; ZrO_2; TiO_2*

■ INTRODUCTION

Titanium dioxide (TiO_2) is a semiconductor that has been widely used as a photocatalyst material because of its interesting properties such as low cost, strong oxidizing power, non-toxicity, and chemical inertness [1]. Another photocatalyst material that has attracted attention is zirconium oxide (ZrO_2) which has good stability and easily produces holes in the valence band, leading to strong interactions with the active component. ZrO_2 is resistant to both alkali and acid conditions as well as oxidation and reduction reactions. Moreover, because of its properties, composites containing ZrO_2 as the main material have pulled much attention in recent years. This is mainly because of the difference in energy levels between ZrO_2 and other semiconductors to efficiently separate the charges, thus decrease the recombination of electrons and holes [2-3].

Previous research reported that coupling ZrO_2 with TiO_2 at Ti:Zr molar ratio of 1:1 had resulted in zirconium titanate hollow sphere with a non-visible-light response (3.31 eV), however, this material has a higher redox potential [1]. Pirzada et al. [2] successfully synthesized nanocomposite TiO_2/ ZrO_2 with the lowest bandgap (3.26 eV, non-visible light response) with an average particle diameter particle of 10.5 nm yielding a higher redox capability. However, the photocatalytic performance of semiconductor can be improved with an approach to broaden the photo-response by doping with various metals [3]. Doping of semiconductor material with transition metals leads to reduction of bandgap and it will provide a good photocatalytic activity [4].

The metallic dopants with 3d orbitals, such as Mn, Fe, Co and Zn, had been studied and reported in recent years [5-9]. Transition metal will reduce the particle size

of photocatalyst and increase its surface area, Table 1 shows the use of dopants with 3d orbitals on the photocatalyst materials that had been studied previously. Doping photocatalyst with transition metals increases the surface defects and optical absorption of light, which can ultimately lead to an increase in the efficiency of the photocatalyst [9]. The lowest bandgap of TiO_2-ZrO_2 doped using Fe (2.83 eV), Co (2.94 eV) and Zn (2.87 eV) were achieved in composites with 7% of iron content calcined at 500 °C, 3% of cobalt content calcined at 500 °C, and 5% of zinc content calcined at 900 °C, respectively [6-8]. The properties of semiconductor are enhanced after manganese doping because Mn^{2+} and Mn^{3+} exist on the surface of photocatalyst and catch the electron in semiconductor. Therefore, Mn should trap electrons and suppress electron–hole recombination. Thus, the lower the electron–hole recombination is, the higher the quantum efficiency of the photons will be and then will reduce bandgap value [10]. Mragui et al. [5] successfully synthesized Mn-TiO_2 with 10% of Mn content and bandgap of 2.95 eV, using $MnCl_2{\cdot}4H_2O$ as a dopant source.

Beside the addition of dopant, the calcination temperature can also affect the bandgap value of the photocatalyst material by changing the structure of the material. TiO_2 which has been synthesized at high calcination (400 °C) could have higher photoactivity compared to the TiO_2 which was synthesized at low temperature (200 °C) [11]. However, photocatalytic activity is related to the combination properties of crystalline phase, particle size, surface area, electron-hole recombinant, bandgap energy, pore volume, and surface chemical state [11-12].

This study was conducted with various Mn dopant contents and calcination temperatures to determine its effects on the properties of Mn-doped TiO_2-ZrO_2 composite. The addition of Mn dopant and increased calcination temperature were expected to produce a TiO_2-ZrO_2 composite with reduced bandgap energy. Mn-doped TiO_2 was developed on the surface of ZrO_2 by the sol-gel process. The sol-gel method was chosen because it has several advantages, such as an easy process, simple equipment, homogeneous phase, the ability to control the crystal size, and low temperature condition [13-14].

Table 1. Bandgap data of Mn-TiO_2, Fe, Co and Zn doped TiO_2-ZrO_2 at the optimum condition

Sample	Eg (eV)
Mn-TiO_2 10% 500 °C	2.95 [5]
Co-ZrO_2-TiO_2 3% 500 °C	2.94 [6]
Fe-ZrO_2-TiO_2 7% 500 °C	2.83 [7]
Zn-ZrO_2-TiO_2 5% 900 °C	2.87 [8]

■ EXPERIMENTAL SECTION

Materials

Titanium(IV) isopropoxide (TTIP, 97%, Sigma-Aldrich) was used as TiO_2 precursor. Manganese(II) chloride tetrahydrate ($MnCl_2{\cdot}4H_2O$, 98%, Merck) was used as source of Mn dopant. Zirconia powder (ZrO_2, Jiaozuo Huasu) was used as the source of coupling semiconductor. Absolute ethanol (Merck) and demineralized water (Jaya Sentosa) were used as solvents.

Instrumentation

Specular reflectance UV-Vis spectrophotometer (SR UV-Vis) UV1700 Pharmaspec was used to measure the ultraviolet and visible (UV-Vis) absorption of the material. Fourier-transform infrared spectroscopy (FTIR) analysis was conducted using Thermo Nicolet iS10. The crystal structures of material were analyzed by using X-ray powder diffractometer (XRD) PANalytical X'Pert PRO MRD instrument with Cu Kα radiation. Surface morphology was observed with scanning electron microscopy equipped with energy dispersive X-ray spectrometer (SEM-EDX) Phenom Desktop ProXL.

Procedure

Mn-doped TiO_2-ZrO_2 was synthesized by the sol-gel method. Firstly, 2.5 mL of TTIP was dissolved in 25 mL of absolute ethanol and then stirred homogeneously. One gram of ZrO_2 powder was dispersed into 25 mL of demineralized water then as much as 14.38, 43.59, 72.66, 101.72, and 130.79 mg of $MnCl_2{\cdot}4H_2O$ was separately added dropwise into the mixture to obtain 1, 3, 5, 7 and 9% Mn wt./Ti wt., respectively. The mixture was stirred for 30 min and separated by centrifugation at 2000 rpm for 1 h. The obtained solid was aged in the open space

for 24 h and then heated at 60 °C for 24 h. Composites with various Mn dopant contents were calcined at 500 °C for 4 h to observe the effect of Mn contents. Additionally, the composite with 5% of Mn content was calcined at 700 and 900 °C to observe the effect of calcination temperature. The variation of dopant percentage and calcination temperature were based on the previous works [6-8]. All samples were characterized by using XRD, FTIR, SR UV-Vis and SEM-EDX.

■ RESULTS AND DISCUSSION

Fig. 1 displays the morphology and its corresponding EDX spectra of 5% Mn-doped TiO_2-ZrO_2 calcined at 500 °C. The morphology of Mn-doped TiO_2-ZrO_2 appears to be rough and its particles appear to be agglomerated with an estimated diameter of 1–5 μm. Table 2 shows the result of EDX spectra analysis. EDX analysis confirms that TiO_2-ZrO_2 was successfully synthesized and 0.33% of Mn was present in the composite.

FTIR spectra of Mn-doped TiO_2-ZrO_2 with various contents of Mn dopant and calcination temperatures are shown together in Fig. 2. FTIR spectra show hydroxyl stretching vibration of H_2O around 3300–3700 cm^{-1} and hydroxyl bending vibration of H_2O around 1650 cm^{-1} [15]. The Zr–O vibration was found around 420 and 744 cm^{-1} correspond to monoclinic structure of ZrO_2 [3]. At low wavenumber region, the absorption belonged to the vibration of Ti–O–Ti, Mn–O–Ti and Mn–O are found around 400–700 cm^{-1} [16]. Spectra of Mn-doped TiO_2-ZrO_2 has combined characteristic vibrations between TiO_2 and ZrO_2, where there are broad stretching vibration

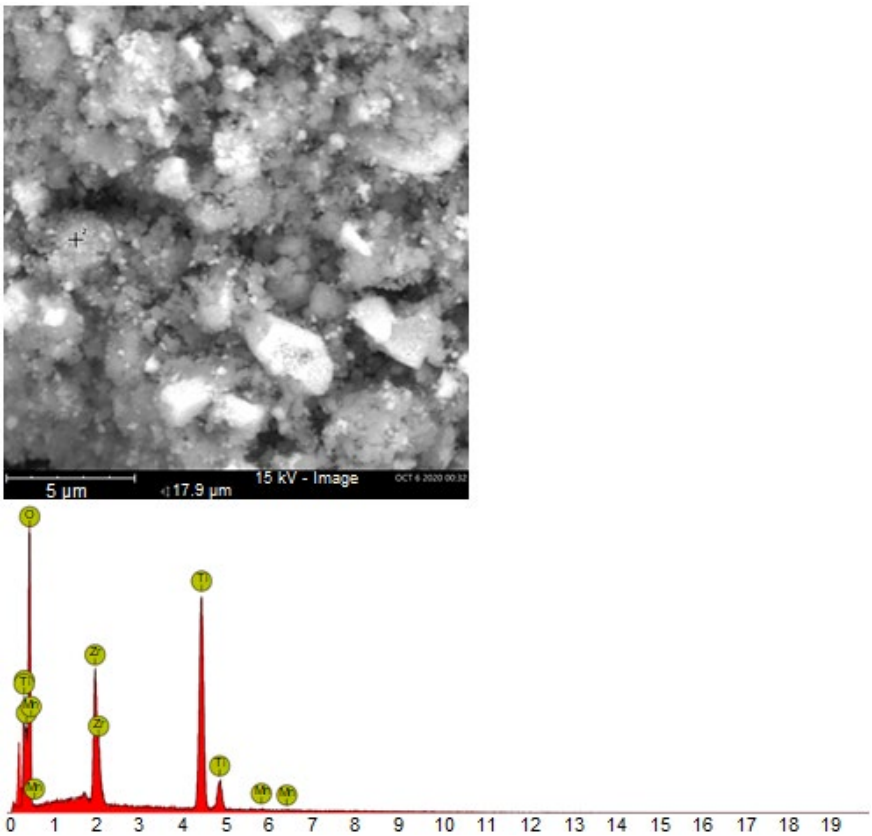

Fig 1. SEM image of TiO_2-ZrO_2 with 5% Mn content calcined at 500 °C and its corresponding EDX spectra

Table 2. EDX analysis of 5% Mn-doped TiO_2-ZrO_2 calcined at 500 °C

Sample	% Weight				
	Zr	Ti	O	Mn	Total
5% Mn-dopedTiO_2-ZrO_2 @ 500 °C	49.09	32.42	18.16	0.33	100

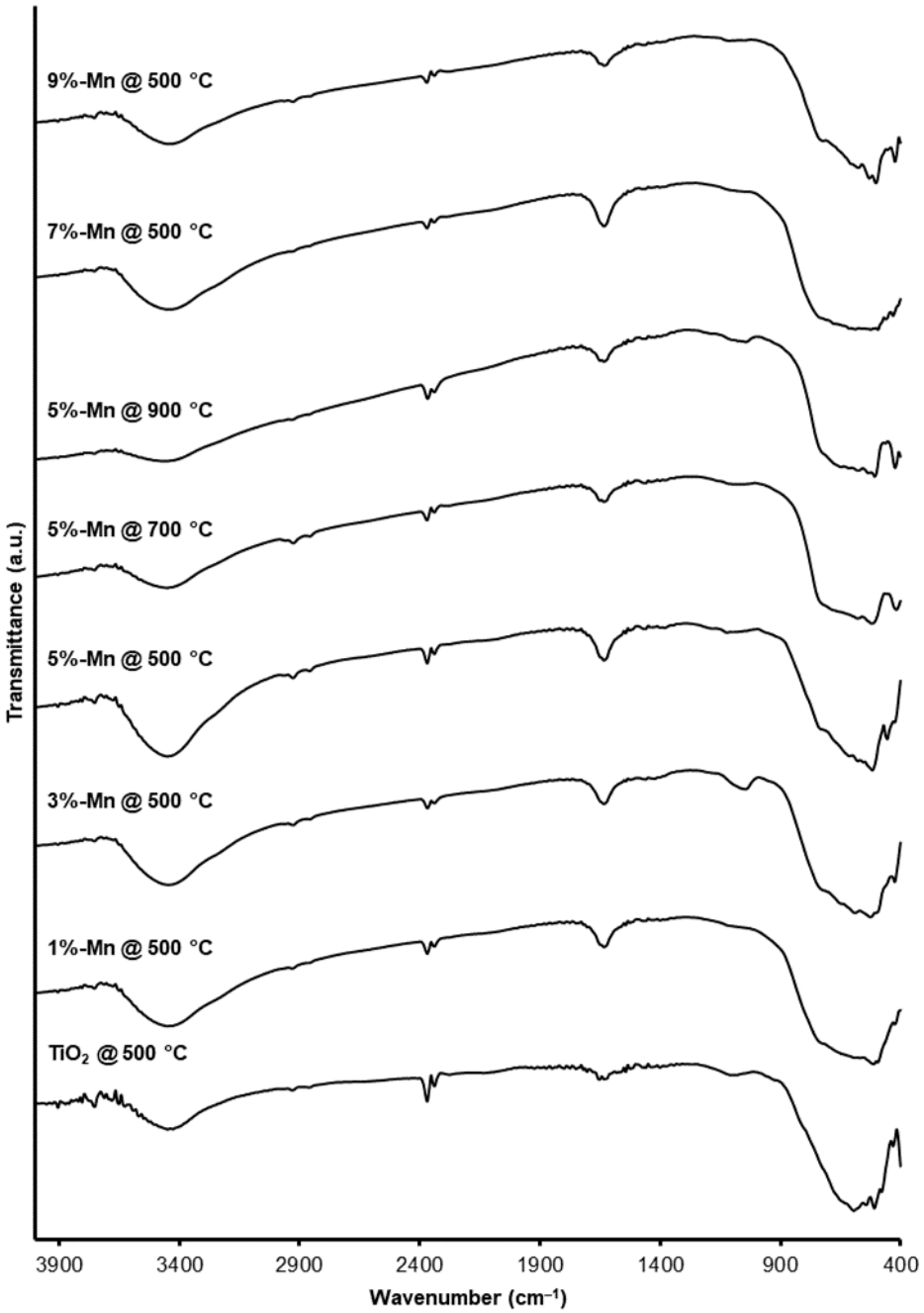

Fig 2. FTIR spectra of Mn-doped TiO_2-ZrO_2 with various dopant contents and calcination temperatures

of OH at 3300–3700 cm^{-1} and also around 400–700 cm^{-1}, which is probably the vibration of Zr–O–Zr, Ti–O–Ti, or Mn–O–Ti. The stretching and bending intensities of H_2O decrease at 9% of Mn-doped TiO_2-ZrO_2, possibly because the number of Mn replacing Ti increases. The hydroxyl bending and stretching intensities of H_2O at 1630 and 3300–3700 cm^{-1}, respectively, decrease with the increase of calcination temperature. This possibly happened because H_2O molecules of synthesized material are released due to the high temperature heating during the calcination process.

Fig. 3 shows diffraction patterns of various Mn-doped TiO_2-ZrO_2 composites, while Table 3 presents their calculated crystallite sizes based on Scherrer's equation [17]. The diffraction patterns confirm the presence of monoclinic ZrO_2 and anatase TiO_2. There are

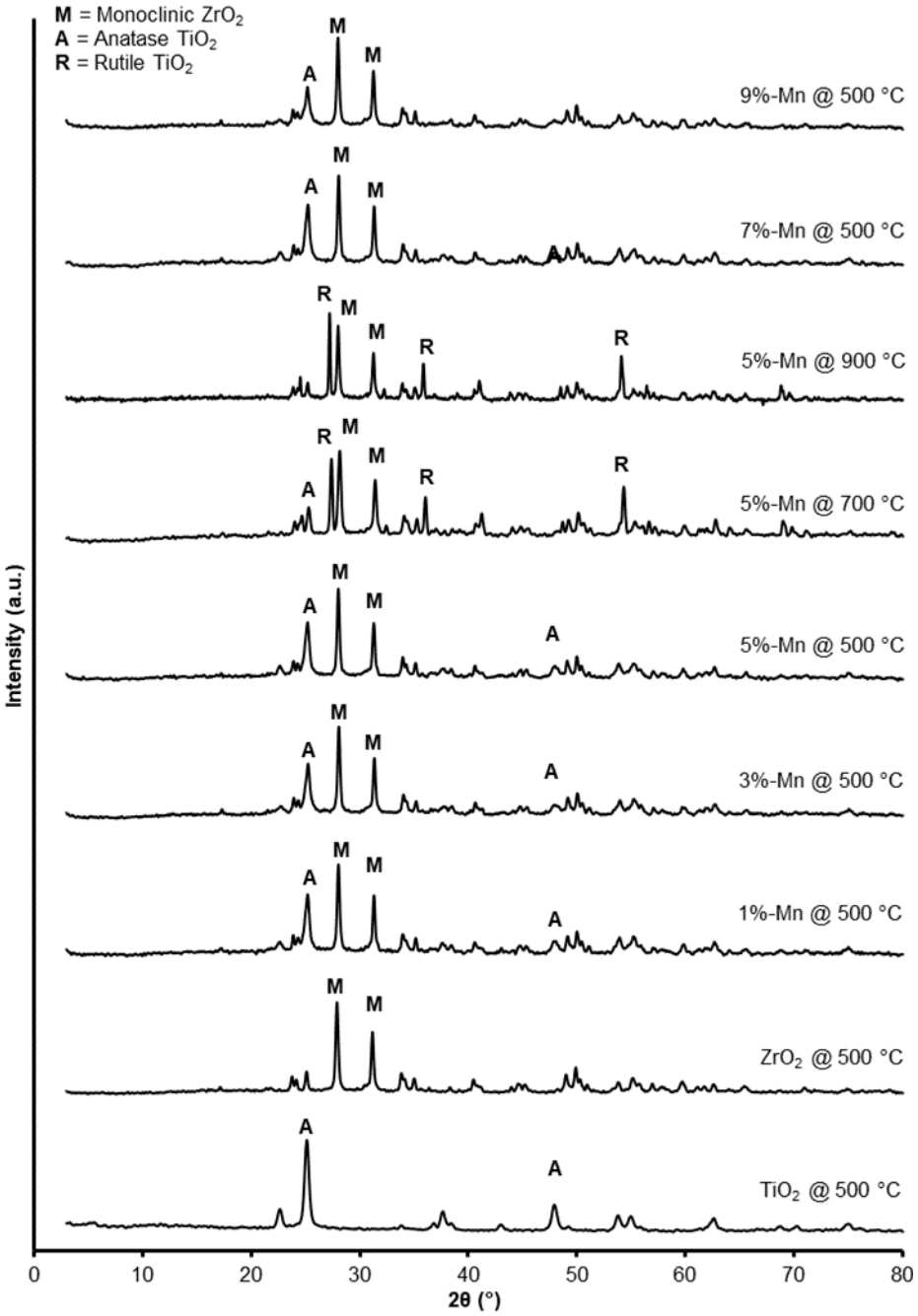

Fig 3. Diffraction patterns of Mn-doped TiO_2-ZrO_2 with various dopant contents and calcination temperatures

no tetragonal and rutile patterns observed at 500 °C. Monoclinic peaks are observed at 28.21° (-111) and 31.50° (111), according to ICDD:01-083-0944, while anatase peaks are observed at 25.28° (101) and 48.05° (200), according to ICDD:00-021-1272. All Mn-doped TiO_2-ZrO_2 had a pattern combination of high monoclinic and anatase intensities at 500 °C, while no Mn pattern was observed. The high intensity of monoclinic peaks shows that ZrO_2 has a greater amount than anatase. The average crystallite sizes of monoclinic and anatase remain unchanged significantly as the content of manganese dopant increases. It indicates that Mn^{2+} (67 pm) has substituted Ti^{4+} (60.5 pm) in the anatase TiO_2 structure, as the ionic radius of both metal ions are similar [18]. Some literature reported that TiO_2 starts to form rutile structure at 500 °C [7,11]. One report found

Table 3. Average crystallite size of various Mn-doped TiO_2-ZrO_2

Sample	Crystal phase	(hkl)	L (nm)
ZrO_2 @ 500 °C	Monoclinic	(-111)	26.36
TiO_2 @ 500 °C	Anatase	(101)	15.72
1%-Mn @ 500 °C	Monoclinic	(-111)	25.10
	Anatase	(101)	15.00
3%-Mn @ 500 °C	Monoclinic	(-111)	27.94
	Anatase	(101)	14.96
5%-Mn @ 500 °C	Monoclinic	(-111)	28.82
	Anatase	(101)	15.60
5%-Mn @ 700 °C	Monoclinic	(-111)	22.88
	Anatase	(101)	18.44
	Rutile	(110)	29.19
5%-Mn @ 900 °C	Monoclinic	(-111)	30.62
	Rutile	(110)	44.64
7%-Mn @ 500 °C	Monoclinic	(-111)	28.28
	Anatase	(101)	15.72
9%-Mn @ 500 °C	Monoclinic	(-111)	29.01
	Anatase	(101)	15.12

that the presence of Mn^{2+} ion promotes anatase-rutile phase transformation [16], while another report suggested that Zr^{4+} prevents phase transformation of anatase [19]. The presence of ZrO_2 is assumed to be responsible for preventing the anatase-to-rutile transformation on Mn-doped TiO_2-ZrO_2 calcined at 500 °C.

The diffraction patterns also confirm the presence of ZrO_2 monoclinic, TiO_2 anatase and TiO_2 rutile at 5% Mn-doped TiO_2-ZrO_2 calcined at 700 and 900 °C. Monoclinic and anatase peaks were observed similar to the previous discussion, but the intensity of anatase decreased while the rutile increased. Rutile peaks are observed at 27.91° (110), 36.43° (101) and 55.11° (211), according to ICDD:01-088-1175 [20]. The intensity of anatase decreased as the calcination temperature increased because of the anatase-to-rutile transformation. The rutile pattern starts to be observed at 700 °C and almost all anatase peaks transform into rutile at 900 °C. The average crystallite size of monoclinic ZrO_2 also remains unchanged at higher calcination temperature. On the other hand, there is an increase in rutile crystallite size, which is possibly due to agglomeration of the rutile phase at 900 °C.

The SR UV-Vis absorption spectra of the Mn-doped TiO_2-ZrO_2 are shown in Fig. 4 with the variation of Mn dopant content and calcination temperature, while Table 4 presents the bandgap energy values. The bandgap energy of the composites was evaluated by using absorption edge cross method. All synthesized materials have lower E_g values than TiO_2 (3.12 eV) and ZrO_2 (3.23 eV) [8,21]. The SR UV-Vis spectra show that all synthesized materials have absorption edge at visible range (above 400 nm). The presence of Mn^{2+} ions forms a new energy orbital under the conduction band and decreases the E_g value of the materials [22]. The increased calcination temperature reduces the E_g values of Mn-doped TiO_2-ZrO_2. This is possibly because the higher calcination temperature would facilitate the phase transformation of anatase to rutile and decrease the E_g value [23].

Based on the obtained results, the synthesized Mn-doped TiO_2-ZrO_2 using the sol-gel method had been successfully carried out. The Mn dopant was proven to reduce the E_g values from 3.12 to 2.78 eV with an optimum content of 5% and calcination temperature of 900 °C. The addition of Mn dopant 1–7% was shown to be able to reduce the E_g value, and it may possibly increase the response of the synthesized material under visible-light range. The E_g values of Mn-doped TiO_2-ZrO_2 increased as the addition of Mn dopant reached above 7%

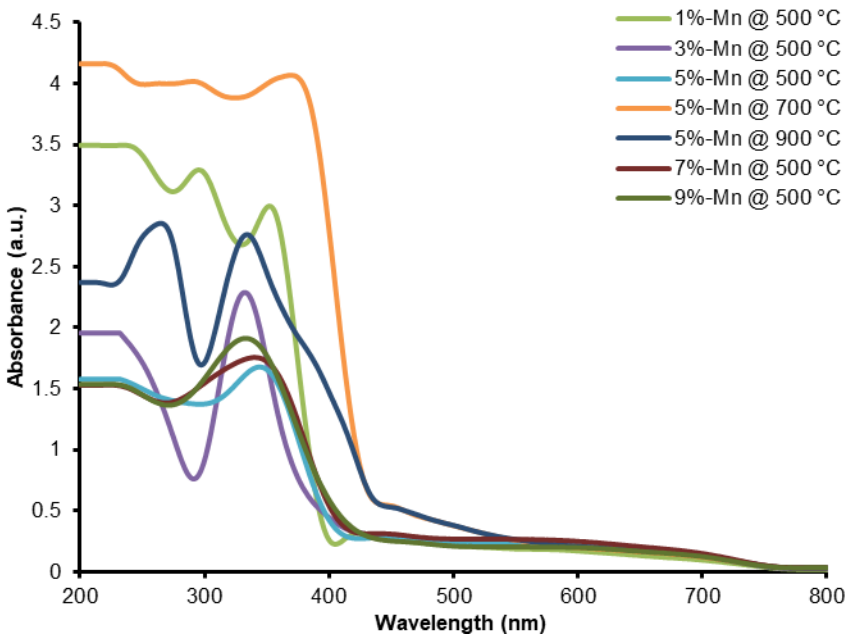

Fig 4. SR UV-Vis absorption spectra of various Mn-doped TiO_2-ZrO_2

Table 4. Bandgap energy data of Mn-doped TiO_2-ZrO_2

Sample	Eg (eV)
1%-Mn @ 500 °C	3.12
3%-Mn @ 500 °C	3.09
5%-Mn @ 500 °C	3.03
5%-Mn @ 700 °C	2.87
5%-Mn @ 900 °C	2.78
7%-Mn @ 500 °C	2.81
9%-Mn @ 500 °C	2.95

due to the heterojunction effect appearing and cancelling the dopant effect [4,6,21]. Furthermore, the higher calcination temperature was proven to enable the material transformations phase of anatase to rutile, which causes the E_g value to be smaller. This result corresponds with other previous works in which the addition of dopant between 1–9% and calcination temperature would show optimum condition of doped composite [4,6-8].

■ CONCLUSION

The investigation of Mn dopant content and calcination temperature affecting the properties of Mn-doped TiO_2-ZrO_2 composite had been successfully conducted. The results of EDX analysis confirm the presence of Zr, Ti, O and Mn. It was confirmed by the XRD analysis that the presence of Zr^{4+} inhibits the anatase-to-rutile transformation at higher calcination temperature. The bandgap of Mn-doped TiO_2-ZrO_2 decreases as the calcination temperature and the dopant content increase until reaching the optimum condition. The composite with the lowest bandgap is Mn-doped TiO_2-ZrO_2 with 5% of Mn content calcined at 900 °C. All of the synthesized composites in this research can be considered as a potential visible-light-responsive photocatalyst.

■ ACKNOWLEDGMENTS

We would like to express our gratitude to The Ministry of Research, Technology and Higher Education of the Republic of Indonesia for their support on this work through PDUPT 2020 Grant (2828/UN1.DITLIT/DIT-LIT/PT/2020).

■ REFERENCES

[1] Syoufian, A., Manako, Y., and Nakashima, K., 2015, Sol-gel preparation of photoactive srilankite-type zirconium titanate hollow spheres by templating sulfonated polystyrene latex particles, *Powder Technol.*, 280, 207–210.

[2] Pirzada, B.M., Mir, N.A., Qutub, N., Mehraj, O., Sabir, S., and Muneer, M., 2015, Synthesis,

characterization and optimization of photocatalytic activity of TiO_2/ZrO_2 nanocomposite heterostructures, *Mater. Sci. Eng., B*, 193, 137–145.

[3] Cheng, Q., Yang, W., Chen, Q., Zhu, J., Li, D., Fu, L., and Zhou, L., 2020, Fe-doped zirconia nanoparticles with highly negative conduction band potential for enhancing visible light photocatalytic performance, *Appl. Surf. Sci.*, 530, 147291.

[4] Deng, Q.R., Xia, X.H., Guo, M.L., Gao, Y., and Shao, G., 2011, Mn-doped TiO_2 nanopowders with remarkable visible light photocatalytic activity, *Mater. Lett.*, 65 (13), 2051–2054.

[5] El Mragui, A., Zegaoui, O., and Daou, I., 2019, Synthesis, characterization and photocatalytic properties under visible light of doped and co-doped TiO_2-based nanoparticles, *Mater. Today: Proc.*, 13, 857–865.

[6] Sulaikhah, E.F., Kurniawan, R., Pradipta, M.F., Trisunaryanti, W., and Syoufian, A., 2020, Cobalt doping on zirconium titanate as a potential photocatalyst with visible-light-response, *Indones. J. Chem.*, 20 (4), 911–918.

[7] Kurniawan, R., Sudiono, S., Trisunaryanti, W., and Syoufian, A., 2019, Synthesis of iron-doped zirconium titanate as a potential visible-light responsive photocatalyst, *Indones. J. Chem.*, 19 (2), 454–460.

[8] Alifi, A., Kurniawan, R., and Syofian, A., 2020, Zinc-doped titania embedded on the surface of zirconia: A potential visible-responsive photocatalyst material, *Indones. J. Chem.*, 20 (6), 1374–1381.

[9] Singh, J., Rathi, A., Rawat, M., Kumar, V., and Kim, K.H., 2019, The effect of manganese doping on structural, optical, and photocatalytic activity of zinc oxide nanoparticles, *Composites, Part B*, 166, 361–370.

[10] Xu, Y., Lei, B., Guo, L., Zhou, W., and Liu, Y., 2008, Preparation, characterization and photocatalytic activity of manganese doped TiO_2 immobilized on silica gel, *J. Hazard. Mater.*, 160 (1), 78–82.

[11] Wu, H., Ma, J., Zhang, C., and He, H., 2014, Effect of TiO_2 calcination temperature on the photocatalytic oxidation of gaseous NH_3, *J. Environ. Sci.*, 26 (3), 673–682.

[12] Lv, K., Xiang, Q., and Yu, J., 2011, Effect of calcination temperature on morphology and photocatalytic activity of anatase TiO_2 nanosheets with exposed {001} facets, *Appl. Catal., B*, 104 (3-4), 275–281.

[13] Tomar, L.J., Bhatt, P.J., Desai, R.k., and Chakrabarty, B.S., 2014, Effect of preparation method on optical and structural properties of TiO_2/ZrO_2 nanocomposite, *J. Nanotechnol. Adv. Mater.*, 2 (1), 27–33.

[14] Wellia, D.V., Xu, Q.C., Sk, M.A., Lim, K.H., Lim, T.M., and Tan, T.T.Y., 2011, Experimental and theoretical studies of Fe-doped TiO_2 films prepared by peroxo sol-gel method, *Appl. Catal., A*, 401 (1-2), 98–105.

[15] Sudrajat, H., Babel, S., Ta, A. T., and Nguyen, T. K., 2020, Mn-doped TiO_2 photocatalysts: Role, chemical identity, and local structure of dopant, *J. Phys. Chem. Solids*, 144, 109517.

[16] Sharotri, N., Sharma, D., and Sud, D., 2019, Experimental and theoretical investigations of Mn-N-co-doped TiO_2 photocatalyst for visible light induced degradation of organic pollutants, *J. Mater. Res. Technol.*, 8 (5), 3995–4009.

[17] Fischer, K., Schulz, P., Atanasov, I., Abdul Latif, A., Thomas, I., Kühnert, M., Prager, A., Griebel, J., and Schulze, A., 2018, Synthesis of high crystalline TiO_2 nanoparticles on a polymer membrane to degrade pollutants from water, *Catalysts*, 8 (9), 376.

[18] Gao, X., Zhou, B., and Yuan, R., 2015, Doping a metal (Ag, Al, Mn, Ni and Zn) on TiO_2 nanotubes and its effect on Rhodamine B photocatalytic oxidation, *Environ. Eng. Res.*, 20 (4), 329–335.

[19] Venkatachalam, N., Palanichamy, M., Arabindoo, B., and Murugesan, V., 2007, Enhanced photocatalytic degradation of 4-chlorophenol by Zr^{4+} doped nano TiO_2, *J. Mol. Catal. A: Chem.*, 266 (1-2), 158–165.

[20] Radić, N., Grbić, B., Petrović, S., Stojadinović, S., Tadić, N., and Stefanov, P., 2020, Effect of cerium oxide doping on the photocatalytic properties of rutile TiO_2 films prepared by spray pyrolysis,

Physica B, 599, 412544.

[21] Andita, K.R., Kurniawan, R., and Syoufian, A., 2019, Synthesis and characterization of Cu-doped zirconium titanate as a potential visible-light responsive photocatalyst, *Indones. J. Chem.*, 19 (3), 761–766.

[22] Abdelouahab Reddam, H., Elmail, R., Lloria, S.C., Monrós Tomás, G., Reddam, Z.A., and Coloma-Pascual, F., 2020, Synthesis of Fe, Mn and Cu modified TiO_2 photocatalysts for photodegradation of Orange II, *Bol. Soc. Esp. Ceram. Vidrio*, 59 (4), 138–148.

[23] Samet, L., Ben Nasseur, J., Chtourou, R., March, K., and Stephan, O., 2013, Heat treatment effect on the physical properties of cobalt doped TiO_2 sol–gel materials, *Mater. Charact.*, 85, 1–12.